RSC Advances

PAPER

Cite this: *RSC Adv.*, 2018, **8**, 14633

Thymoquinone protects against cardiac damage from doxorubicin-induced heart failure in Sprague-Dawley rats

Zuowei Pei,[a] Jiahui Hu,[ab] Qianru Bai,[ab] Baiting Liu,[c] Dong Cheng,[a] Hainiang Liu,[a] Rongmei Na[a] and Qin Yu*[a]

Heart failure is a complex end stage result of various cardiovascular diseases, and has a poor prognosis. The mechanisms for the development and progression of heart failure have always been an important topic in cardiovascular research, and previous studies have shown that thymoquinone (TQ) protects against cardiotoxicity and cardiac damage. The aim of this study was to investigate the possible protective effects of thymoquinone against cardiac damage in doxorubicin (DOX)-induced heart failure in Sprague-Dawley Rats (SDR). Forty-five male SDR were randomly divided into three groups and administered different treatment regimens for 8 weeks. Left ventricular fractional shortening (LVFS) and ejection fraction (LVEF) were higher in the DOX + TQ group than those in the DOX group. Significant pathophysiology changes (HE and Masson staining) were observed in rats of the DOX group compared to those of the DOX + TQ group. The addition of Thymoquinone inhibited DOX-induced cardiac fibrosis (TGF-β, Smad3, collagen I, collagen III, and α-SMA) and apoptosis (P53, bcl-2, caspase-3, caspase-9, and BAX) in SDR, indicating that thymoquinone may be a potential therapeutic target for cardiac damage caused by DOX-induced heart failure.

Received 31st January 2018
Accepted 26th March 2018

DOI: 10.1039/c8ra00975a

rsc.li/rsc-advances

Introduction

Cardiovascular diseases, particularly heart failure (HF), are the most common cause of human death worldwide.[1] In China, there are over 4 million patients with HF and the mortality rate in these patients is much higher than that in developed countries.[2] In the treatment of cancer, the antineoplastic drug doxorubicin is effective in treating a broad spectrum of malignancies, but its clinical use is limited by adverse side effects including severe cardiotoxicity, which can lead to progressive and irreversible HF.[3,4] There is increasing evidence that programmed myocardial fibrosis cell death, or apoptosis, contributes substantially to the pathogenesis of HF.[5–7] To date, however, available treatments to protect against cardiac damage from doxorubicin (DOX)-induced HF have been varied and limited.

Herbal medicine has attracted much attention in recent years and is increasingly used to offer an alternative to chemical drugs. Several lines of evidence support the positive effects of medicinal plants in the prevention and cure of a wide range of diseases. Thymoquinone (TQ) is one of these compounds. It is the main active ingredient of *Nigella sativa*, commonly known as black cumin or black seed, an annual flowering plant native to some areas such as the Mediterranean countries.[8] Since its first extraction in 1963,[9] thymoquinone has been shown to have anti-fibrotic and anti-apoptosis properties both *in vivo* and *in vitro*.[10–14] The aim of this study was to determine the role of thymoquinone in doxorubicin-induced cardiac damage. Our results will contribute to wider understanding of the beneficial role and mechanism of thymoquinone in doxorubicin-induced HF.

Materials and methods

DOX-induced heart failure model

Sprague-Dawley Rats (SDR) were provided by the Dalian Medical University Laboratory Animal Center. All animals were housed under diurnal lighting conditions and allowed food and water ad libitum. The animal model was established based accepted the methods previously described.[15,16] Forty-five male SDR weighing 150 ± 20 g were randomly divided into three groups: a control group (normal saline, NS, $n = 15$), a DOX group ($n = 15$) and a DOX + TQ group ($n = 15$). Heart failure was induced experimentally by intraperitoneal injections of the cardiotoxic agent doxorubicin (DOX) at a cumulative dose of 15 mg kg^{-1} in 6 injections (DOX, 2.5 mg kg^{-1} × 6) over a 2 week period. 30 SDR received DOX injections, and following this, 15/30 received further tube feeding

[a]*Department of Cardiology, Affiliated Zhongshan Hospital of Dalian University, No. 6 Jiefang Street, Dalian, 116001, China. E-mail: yuqin@dlu.edu.cn; Fax: +86-0411-62893517; Tel: +86-0411-62893517*

[b]*Graduate School of Dalian Medical University, No. 9 Lvshun South Road, Dalian, China*

[c]*International Medical Department, Affiliated Zhongshan Hospital of Dalian University, No. 6 Jiefang Street, Dalian, China*

of 50 mg kg^{-1} d^{-1} of TQ (purity ≥ 98%; Sigma-Aldrich, St. Louis, MO, USA) over 8 weeks. All animal procedures were performed in accordance with the Guidelines for Care and Use of Laboratory Animals of Dalian University and approved by the Animal Ethics Committee of Affiliated Zhongshan Hospital of Dalian University.

Echocardiographic examination

The rats were anaesthetised with 2.5% isoflurane in 95% oxygen and 5% carbon dioxide, and hair on the chest was removed by shaving and with animal depilatory cream which produced such as Nair®. Left ventricular function was evaluated by echocardiography using a high-resolution small animal imaging system (Vevo 2100; VisualSonics Inc., Toronto, Canada), with the animal placed in the supine position on a warming platform. Two-dimensional and M-mode echocardiographic studies were performed from short axis view and end-systolic and ventricular dimensions.[17] Left ventricular function was assessed using the following parameters: ejection fraction (EF), fractional shortening (FS), left ventricular diastolic and systolic diameters (LVEDD and LVESD).

Haematoxylin-eosin staining

The cardiac tissues were fixed with 10% buffered formalin solution for 30 minutes and then dehydrated in 75% ethanol overnight, followed by paraffin embedding. For morphometric analysis of atherosclerotic lesions, serial 4 μm sections were cut. The sections were stained with haematoxylin and eosin for histologic analysis.

Masson's trichrome staining

Rat heart tissue from each group was stored in 10% formalin for 2 weeks, dehydrated in an ascending series of alcohols (75%, 85%, 90%, and 100% alcohol, 5 min each) and embedded in paraffin wax. The 4 μm-thick paraffin sections were sliced from these paraffin-embedded tissue blocks. Tissue sections were deparaffinised *via* immersion in xylene (3 times, for 5 min each) and rehydrated using a descending series of alcohols (100%, 90%, 85%, and 75% alcohol, 5 min each). Biopsy samples were stained using Masson's trichrome stain to investigate any morphological and fibrotic changes in the heart. Blue staining represented collagen accumulation. The results were visualised using an Olympus B×40 upright light microscope (Olympus, Tokyo, Japan).

Immunohistochemistry analysis

Immunohistochemistry was performed using the Histone Simple stain kits (Nichirei, Tokyo, Japan) according to the manufacturer's instructions. Briefly, paraffin-embedded sections were deparaffinised with xylene and then rehydrated in a descending series of ethanol concentrations. The sections were treated for 15 min with 3% H_2O_2 in methanol to inactivate endogenous peroxidases and were then incubated at room temperature for 1 h with the primary antibodies against caspase-3 (rabbit anti-caspase-3 antibody, 1 : 500; Abcam, England); caspase-9 (rabbit anti-caspase-9 antibody, 1 : 500; Abcam) and BAX (rabbit anti-BAX antibody, 1 : 500; Cell Signaling Technology). All sections were analysed using an Olympus B×40 upright light microscope (Olympus, Tokyo, Japan). For each staining, a total of 3 × 7 sections (7 rats) per group were analysed and the representative images were presented. All image analyses were undertaken by a blinded reviewer.

Western blot analysis

The cardiac tissues were harvested, and protein extracts prepared, according to established methods. Extracts were separated in sodium dodecyl sulphate–polyacrylamide electrophoresis gels (8–15%) and transferred to a polyvinylidene difluoride (PVDF) membrane (Millipore, Bedford, MA, USA). The membranes were blocked with 5% milk and then incubated with indicated primary antibodies at 4 °C overnight. Primary antibodies against TGF-β (rabbit anti-TGF-β antibody, 1 : 1000; Proteintech, Wuhan, China), Smad3 (rabbit anti-Smad antibody, 1 : 1000; Proteintech), collagen I (rabbit anti-collagen I antibody, 1 : 1000; Proteintech), collagen III (rabbit anti-collagen III antibody, 1 : 1000; Proteintech), α-SMA (rabbit anti-α-SMA antibody, 1 : 1000; Proteintech), P53 (rabbit anti-P53 antibody, 1 : 1000; Proteintech), bcl-2(rabbit anti-bcl-2 antibody, 1 : 1000; Proteintech), anti-β-actin (1 : 1000; Cell Signaling Technology). After washing, the membranes were incubated with the appropriate secondary antibody (anti-rabbit Ig-G, 1 : 1000; Cell Signaling Technology) for 1 hour. This analysis was carried out independently three times. Protein levels were expressed as protein/β-actin ratios to minimise loading differences. The relative signal intensity was quantified using NIH ImageJ software.

Statistical analysis

All data are presented as the mean ± SEM. Statistical analysis was performed using SPSS software version 23.0 (SPSS Inc., Chicago, IL, USA). Inter-group variation was measured by one-way ANOVA and subsequent Tukey's test. The minimal level for statistical significance was $p < 0.05$.

Table 1 Metabolic characteristics of three group rats with 8 weeks treatment[a]

	Control group ($n = 13$)	DOX group ($n = 9$)	DOX + TQ group ($n = 12$)
Heart weight (mg)	992.34 ± 41.73	916.18 ± 34.62	912.07 ± 37.53
Body weight (g)	368.57 ± 17.48	279.62 ± 5.07*	290.71 ± 13.07*
Heart/body weight (mg g^{-1})	2.71 ± 0.19	3.14 ± 0.25	3.02 ± 0.21

[a] Data are given as the means ± SEM; $n = 9$–13 in each group. *$P < 0.05$ *vs.* Control group.

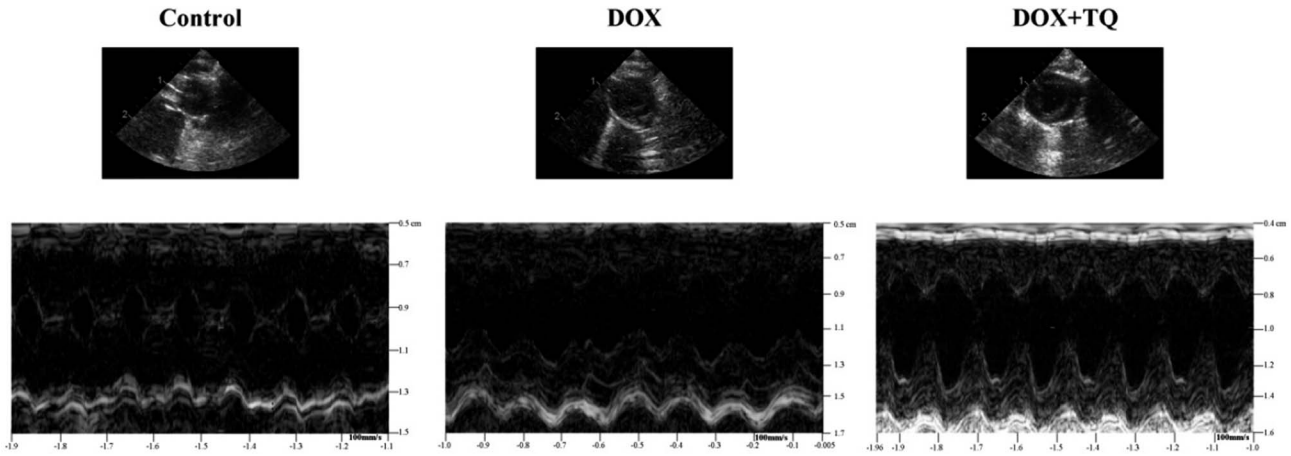

Fig. 1 Representative M-mode echocardiographic tracings.

Table 2 Echocardiographic characteristics of three group rats with 8 weeks treatment[a]

	Control group ($n = 13$)	DOX group ($n = 9$)	DOX + TQ group ($n = 12$)
LVEF (%)	95.63 ± 3.89	63.67 ± 3.09*	87.13 ± 2.09**
LVFS (%)	66.5 ± 2.35	30.63 ± 4.16*	54.5 ± 2.62**
LVESD (mm)	1.5 ± 0.13	2.68 ± 0.17*	2.44 ± 0.2*
LVEDD (mm)	3.82 ± 0.22	4.67 ± 0.12*	4.24 ± 0.22*

[a] LVEF = left ventricular ejection fraction; LVFS = left ventricular fractional shortening; LVEDD = left ventricular end-diastolic dimension; LVESD = left ventricular end-systolic dimension. Data are given as the means ± SEM; $n = 9$–13 in each group. *$P < 0.05$ *vs.* Control group; **$P < 0.05$ *vs.* DOX group.

Results

Metabolic characterisation

The metabolic characteristics of SDR after 8 weeks of different treatments are summarised in Table 1. Heart weights and heart/body weights did not differ among the three groups although the body weights of DOX and DOX + TQ groups showed significantly decreased values compared with those of the control group.

Thymoquinone suppressed DOX-induced cardiac left ventricular function damage

M-mode echocardiography was used to assess cardiac dimensions. LVEF and LVFS were significantly decreased in the DOX group compared to those of the control group; however, the decrease in the DOX group was greater with the addition of TQ. LVESD and LVEDD were significantly increased in both the DOX and DOX + TQ groups compared to those in the control group, but did not differ significantly between the DOX and the DOX + TQ groups (Fig. 1 and Table 2). These results suggest that TQ can protect cardiac function in DOX-induced cardiac damage.

Histopathological changes in the cardiac tissues

The HE staining results showed significant histopathological changes in rats of the DOX group compared to those in rats of the control group: some parts appeared enlarged, showed signs of degeneration, evidence of dissolution or necrosis of myocardial cells, myofibril twist, inflammatory cell infiltration, and

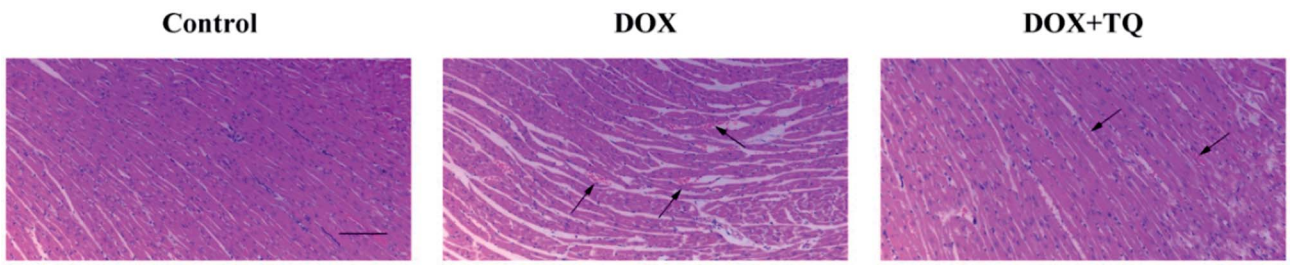

Fig. 2 Effect of TQ on DOX-induced histopathological changes in the cardiac tissues. Histopathological changes were evaluated by HE staining ($n = 5$). Scale bar = 200 μm. Arrows indicate positively stained cells.

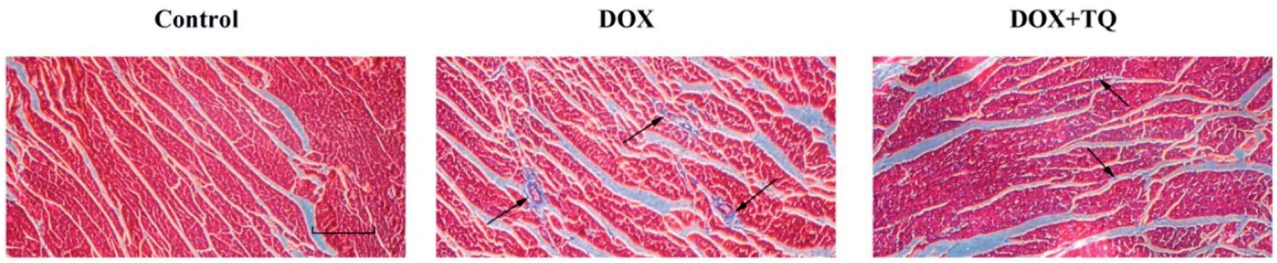

Fig. 3 Effect of TQ on DOX-induced left ventricular myocardial fibrosis. Fibrosis was evaluated by Masson's trichrome staining ($n = 5$), with myocardial cells stained red, and collagenous fibres stained blue. Scale bar = 200 μm. Arrows indicate positively stained cells.

myocardial fibre rupture. Most lesions were absorbed in the DOX + TQ groups; individuals still showed a small amount of inflammatory cell infiltration (Fig. 2).

Thymoquinone inhibited DOX-induced myocardial collagen deposition

To evaluate collagen deposition in the left ventricle, Masson's trichrome staining was used to stain myocardial cells red and collagenous fibres blue (Fig. 3). Compared with the control group, the DOX group showed widespread fibrous tissue in interstitial and perivascular areas, however, rats treated with TQ after DOX-induced cardiac damage exhibited considerably less fibrous tissue, suggesting that TQ can attenuate myocardial fibrosis.

Thymoquinone inhibited DOX-induced cardiac fibrosis

To investigate the mechanism underlying the antifibrotic effects of TQ, protein levels of TGF-β, Smad3, collagen I, collagen III, and α-SMA in the cardiac tissues were determined by western blotting. Our results showed the TGF-β, Smad, collagen I, collagen III, and α-SMA protein levels in DOX + TQ group rats were significantly suppressed compared to those in the DOX group (Fig. 4).

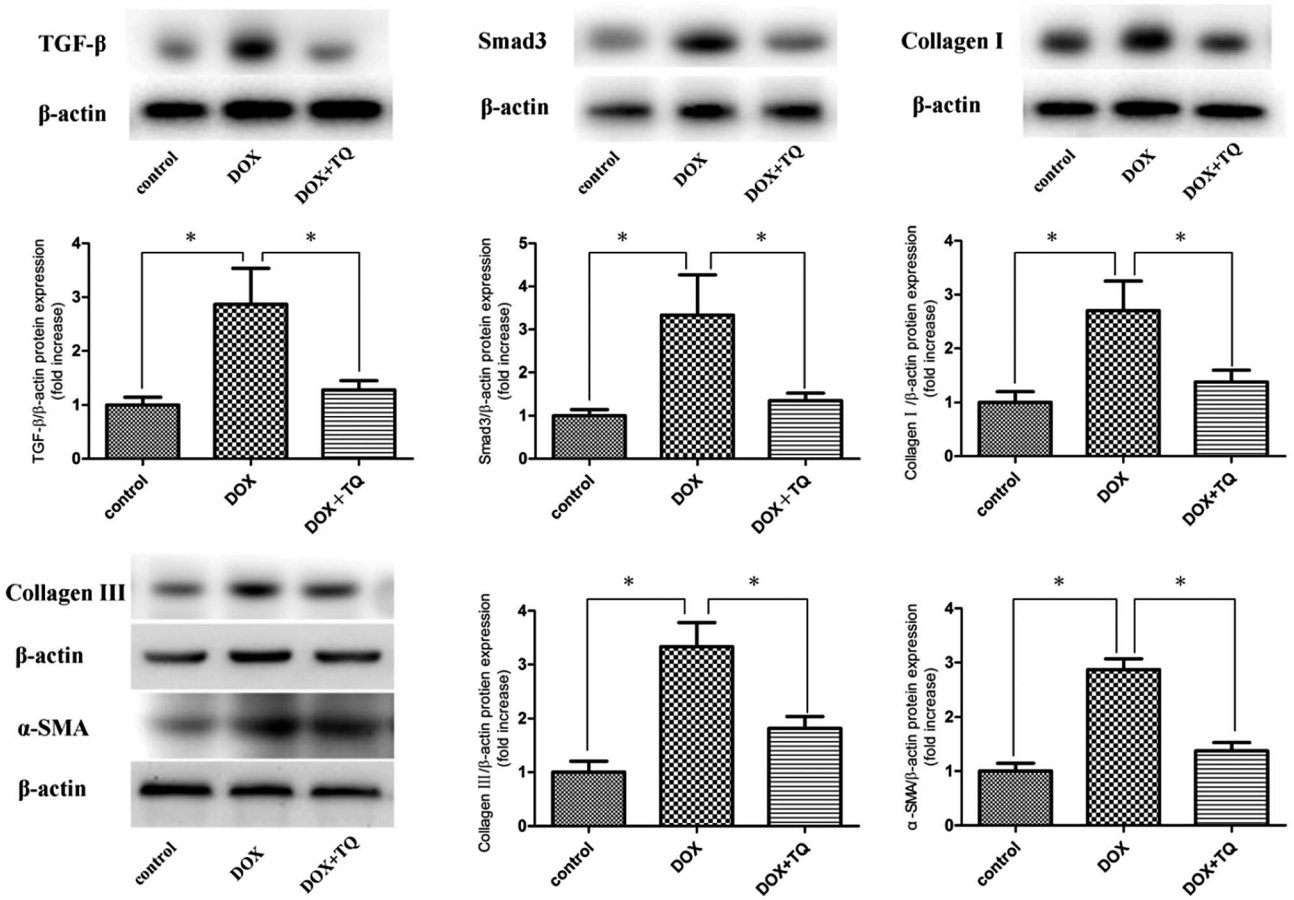

Fig. 4 Protein levels of TGF-β, Smad3, collagen I, collagen III, and α-SMA in cardiac tissue were determined by western blotting. Immunoblotting for TGF-β, Smad3, collagen I, collagen III, and α-SMA in cardiac tissues. Bar graph showing quantification of TGF-β, Smad3, collagen I, collagen III, and α-SMA protein expression. Data are given as the mean ± SEM; $n = 3$ in each group. *$p < 0.05$ *vs.* DOX group.

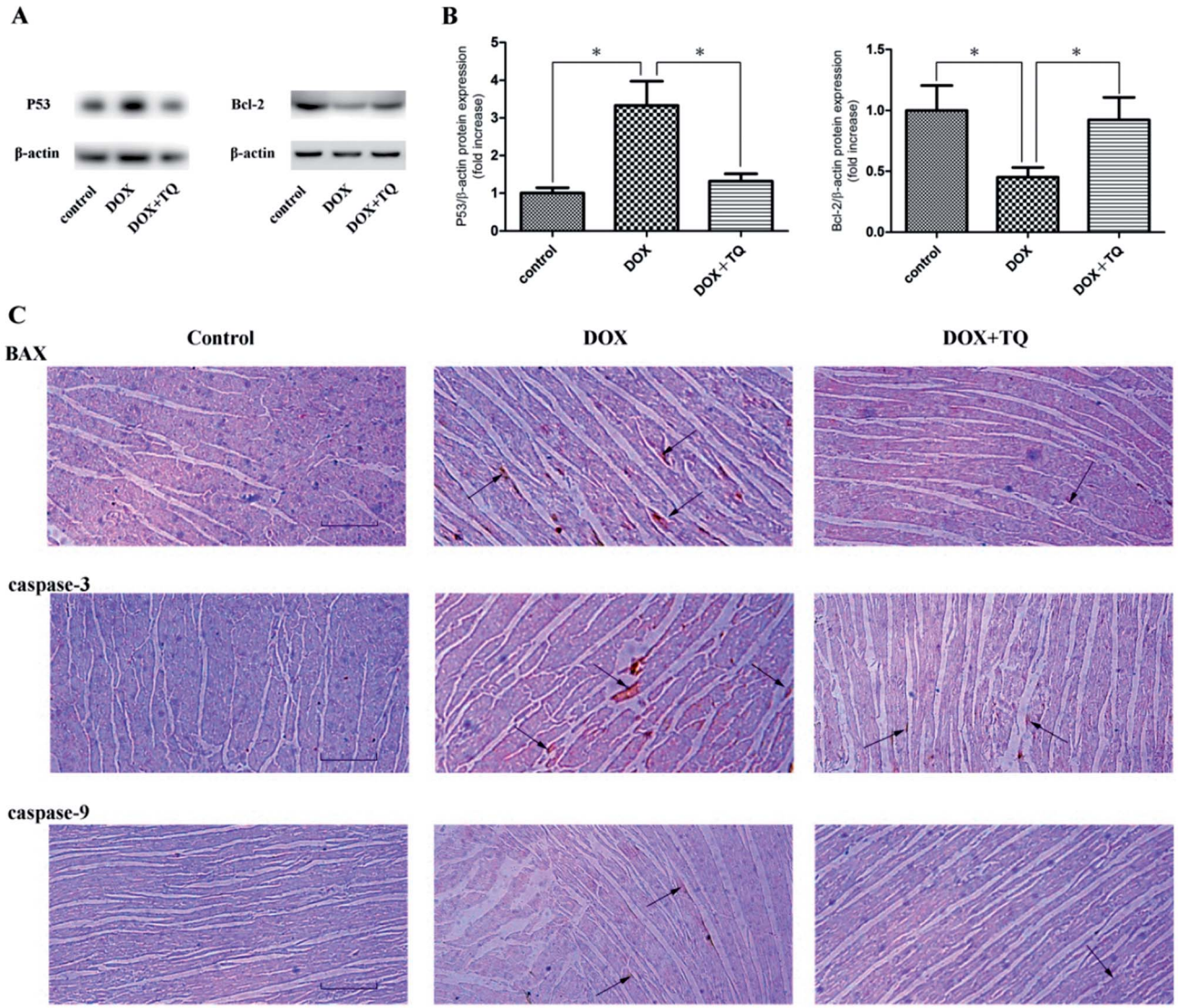

Fig. 5 P53, bcl-2, caspase-3, caspase-9, and BAX expression in the cardiac tissues of all groups after 8 weeks with different treatments. (A) Immunoblotting for p53 and bcl-2 in cardiac tissues. (B) Bar graph showing quantification of p53 and bcl-2 protein expression. Data are given as the mean ± SEM; $n = 3$ in each group. *$p < 0.05$ *vs.* DOX group. (C) Representative immunohistochemistry staining for caspase-3, caspase-9, and BAX expression in cardiac tissues. Scale bar = 200 μm. Arrows indicate positively stained cells.

Thymoquinone suppressed DOX-induced myocardial apoptosis

To detect myocardial apoptosis, immunoblotting analysis using P53 and bcl-2, and immunohistochemical analysis using caspase-3, caspase-9, and BAX were performed (Fig. 5). The rats in the DOX + TQ group showed a markedly reduced caspase-3-, caspase-9-, and BAX-positive staining in the cardiac tissues compared to that in the DOX group. These results indicate that thymoquinone reduced myocardial apoptosis in the DOX rats.

Discussion

This study showed that thymoquinone has a protective effect against cardiac damage, especially left ventricular function damage, myocardial fibrosis and apoptosis by DOX-induced heart failure.

Regarding metabolic characteristics, we found that heart weights and heart/body weights did not differ among the three groups; body weights in the DOX and DOX + TQ groups showed significantly lower values than those of the control group. These results suggest that, although DOX significantly affects body weight, the TQ treatment did not make any difference.

According to the echocardiographic examination, TQ may increase LVEF and LVFS, leading to an improvement in left ventricular function in the DOX-induced rat HF model. Pathophysiological changes were significantly reduced in the DOX + TQ group compared to those in the DOX group, determined using HE staining.

An increase in synthesis or decrease in degradation of myocardial collagen serves an important role in cardiac damage following HF, which ultimately affects left ventricular function. This study demonstrated that myocardial collagen deposition in the HF group was significantly higher than that in the control

group, indicating that myocardial fibroblasts proliferate, leading to increased synthesis and secretion of collagen as well as remodelling of the cardiac collagen spatial network. However, reduction in the TQ treatment group indicated that myocardial collagen deposition decreased.

TGF-β is an important signalling molecule that induces cardiac fibrosis by activating the proliferation and collagen production of cardiac fibroblasts.[18] Previous studies have investigated TGF-β-induced ECMR and fibrosis in various diseases, including cardiac fibroblast–myofibroblast transition.[19–21] Several lines of evidence suggest a role for excessive TGF-β signalling in the pathogenesis of maladaptive remodelling and fibrosis. TGF-β binds to receptors and induces a number of responses, including the upregulation of mesenchymal-associated proteins, such as collagen and α-SMA.[22] TGF-β/Smads is known to be a classical cell signalling pathway during disease progression. Recent studies suggest that the TGF-β/Smads signalling pathway plays a crucial role in the pathogenesis of cardiac fibrosis.[23] Our results concur with these reports, showing that TGF-β, Smad3, α-SMA, collagen I, and collagen III protein expression levels were significantly reduced in the DOX + TQ group compared to those in the DOX group rats.

It has been reported that the occurrence of HF is not only caused by the reduction in cardiac fibrosis, but also by an increase in the percentage of apoptotic cells. Apoptosis plays a critical role in the process of ventricular remodelling and heart failure.[24–26] The Bcl-2 protein family determines the commitment of cells to apoptosis and activation of caspase-3 triggers the execution of cell apoptosis. In the Bcl-2 protein family, there are both pro-apoptotic proteins and anti-apoptotic proteins. Bax, in the form of oligomers, can prompt the formation of membrane pores and release pro-apoptotic substances into the cytoplasm, exerting pro-apoptotic function. Conversely, Bcl-2 inhibits cell apoptosis by blocking oligomerisation of pro-apoptotic proteins.[27] In addition, P53 is closely related to the apoptotic pathway; it can not only upregulate Bax expression, but may also directly interact with Bcl-2 in order to inhibit any anti-apoptotic effect.[28] Our study showed that P53, Bax, caspase-3, and caspase-9 expression levels were significantly reduced in the DOX + TQ group compared to those in the DOX group rats. However, bcl-2 protein expression significantly increased in the DOX + TQ group compared to that in the DOX group. These results indicate that thymoquinone reduces cardiac fibrosis in SDR in the DOX-induced HF group.

Our study establishes that thymoquinone contributes to the mitigation of DOX-induced cardiac damage as shown by the improved left ventricular function, suppressed myocardial fibrosis, and apoptosis. These findings provide new insights into the role of thymoquinone in DOX-induced cardiac damage and raise the possibility of a novel therapeutic intervention for the treatment of cardiovascular diseases progression.

Author contributions

Qin Yu designed this study; Zuowei Pei, Jiahui Hu and Qianru Bai helped in performing experiments; Qin Yu and Zuowei Pei analyzed data and interpreted the results of experiments; Rongmei Na and Baiting Liu prepared figures; Zuowei Pei drafted the manuscript; Dong Cheng and Hainiang Liu helped to revising of manuscript. All authors read and approved the final manuscript.

Conflicts of interest

The authors declare no conflict of interest.

Acknowledgements

This work was finally supported by the National Natural Science Foundation of China (No. 81770405).

References

1 D. Lloyd-Jones, R. Adams, M. Carnethon, S. G. De, T. B. Ferguson and K. Flegal, Heart disease and stroke statistics–2009 update: a report from the American Heart Association Statistics Committee and Stroke Statistics Subcommittee, *Circulation*, 2009, **119**, 480–486.

2 A. S. Go, D. Mozaffarian, V. L. Roger, E. J. Benjamin and J. D. Berry, Heart disease and stroke statistics–2013 update: a report from the American Heart Association. American Heart Association Statistics Committee and Stroke Statistics Subcommittee, *Circulation*, 2013, **127**, 143–152.

3 R. D. Olson and P. Mushlin, Doxorubicin cardiotoxicity: analysis of prevailing hypotheses, *FASEB J.*, 1990, **4**, 3076–3086.

4 P. K. Singal and N. Iliskovic, Doxorubicin-induced cardiomyopathy, *N. Engl. J. Med.*, 1998, **339**, 900–905.

5 V. V. Petrov, R. H. Fagard and P. J. Lijnen, Stimulation of collagen production by transforming growth factor-beta1 during differentiation of cardiac fibroblasts to myofibroblasts, *Hypertension*, 2002, **39**, 258–263.

6 J. Narula, N. Haider, E. Arbustini and Y. Chandrashekhar, Mechanisms of disease: apoptosis in heart failure: seeing hope in death, *Nat. Clin. Pract. Cardiovasc. Med.*, 2006, **3**, 681–688.

7 G. W. Dorn II, Apoptotic and non-apoptotic programmed cardiomyocyte death in ventricular remodelling, *Cardiovasc. Res.*, 2009, **81**, 465–473.

8 H. Gali-Muhtasib and A. Roessner, Thymoquinone: a promising anti-cancer drug from natural sources, *Int. J. Biochem. Cell Biol.*, 2006, **18**, 1249–1253.

9 M. El-Dakhakhny, Studies on the chemical constitution of Egyptian N. sativa L. seeds, *Planta Med.*, 1963, **11**, 465–470.

10 T. Bai, L. H. Lian, L. Wu, Y. Wan and J. X. Nan, Thymoquinone attenuates liver fibrosis *via* PI3K and TLR4 signaling pathways in activated hepatic stellate cells, *Int. Immunopharmacol.*, 2013, **15**, 275–281.

11 T. Bai, Y. Yang, Y. L. Wu, S. Jiang, J. J. Lee and L. H. Lian, Thymoquinone allevi-ates thioacetamide-induced hepatic fibrosis and inflammation by activating LKB1-AMPK signaling pathway in mice, *Int. Immunopharmacol.*, 2014, **19**, 351–357.

12 A. Singh, I. Ahmad, S. Akhter, G. K. Jain, Z. Iqbal and S. Talegaonkar, Nanocar-rier based formulation of thymoquinone improves oral delivery: stability assessment, *in vitro* and *in vivo* studies, *Colloids Surf., B*, 2013, **102**, 822–832.

13 A. Paramasivam, S. Sambantham, J. Shabnam, S. Raghunandhakumar, B. Anandan and A. Rajiv, Anti-cancer effects of thymoquinone in mouse neuroblastoma (Neuro-2a) cells through caspase-3 activation with down-regulation of XIAP, *Toxicol. Lett.*, 2012, **213**, 151–159.

14 X. Lei, X. Lv, M. Liu, Z. Yang, M. Ji and X. Guo, Thymoquinone inhibits growth and augments 5-fluorouracil-induced apoptosis in gastric cancer cells both *in vitro* and *in vivo*, *Biochem. Biophys. Res. Commun.*, 2012, **417**, 864–868.

15 P. J. Lee, D. Rudenko, M. A. Kuliszewski, C. Liao, M. G. Kabir, K. A. Connelly and H. Leong-Poi, Survivin gene therapy attenuates left ventricular systolic dysfunction in doxorubicin cardiomyopathy by reducing apoptosis and fibrosis, *Cardiovasc. Res.*, 2014, **3**, 423–433.

16 H. I. Ammar, S. Saba, R. I. Ammar, L. A. Elsayed, W. B. Ghaly and S. Dhingra, Erythropoietin protects against doxorubicin-induced heart failure, *Am. J. Physiol.: Heart Circ. Physiol.*, 2011, **6**, 2413–2421.

17 G. Condorelli, C. Morisco, G. Stassi, A. Notte, F. Farina, G. Sgaramella, A. de Rienzo, R. Roncarati, B. Trimarco and G. Lembo, Increased cardiomyocyte apoptosis and changes in proapoptotic and antiapoptotic genes bax and bcl-2 during Left ventricular adaptations to chronic pressure overload in the rat, *Circulation*, 1999, **99**, 3071–3078.

18 M. Bujak and N. G. Frangogiannis, The role of TGF-beta signaling in myocardial infarction and cardiac remodeling, *Cardiovasc. Res.*, 2007, **74**, 184–195.

19 Z. Tao, Y. Ge, N. Zhou, Y. Wang, W. Cheng and Z. Yang, Puerarin inhibits cardiac fibrosis *via* monocyte chemoattractant protein (MCP)-1 and the transforming growth factor-β1 (TGF-β1) pathway in myocardial infarction mice, *Am. J. Transl. Res.*, 2016, **8**, 4425–4433.

20 D. Gonzalez, O. Contreras, D. L. Rebolledo, J. P. Espinoza, B. Van Zundert and E. Brandan, ALS skeletal muscle shows enhanced TGF-β signaling, fibrosis and induction of fibro/adipogenic progenitor markers, *PLoS One*, 2017, **12**, e0177649, DOI: 10.1371/journal.pone.0177649.

21 W. Liu, X. Wang, Z. Mei, J. Gong, L. Huang, X. Gao, Y. Zhao, J. Ma and L. Qian, BNIP3L promotes cardiac fibrosis in cardiac fibroblasts through $[Ca^{+}]$i-TGF-β-Smad2/3 pathway, *Sci. Rep.*, 2017, **7**, 1906, DOI: 10.1038/s41598-017-01936-5.

22 X. Chen, J. Xu, B. Jiang and D. Liu, Bone morphogenetic protein-7 antagonizes myocardial fibrosis induced by atrial fibrillation by restraining transforming growth factor-β (TGF-β)/Smads signaling, *Med. Sci. Monit.*, 2016, **22**, 3457–3468.

23 J. Ni, Y. Shi, L. Li, J. Chen, L. Li, M. Li and J. Zhu, Cardioprotection against Heart Failure by Shenfu Injection *via* TGF-β/Smads Signaling Pathway, *J. Evid. Based Complementary Altern. Med.*, 2017, **2017**, 1–16.

24 K. Emanuel, U. Mackiewicz, B. Pytkowski and B. Lewartowski, Properties of ventricular myocytes isolated from the hypertrophied and failing hearts of spontaneously hypertensive rats, *J. Physiol. Pharmacol.*, 1999, **50**, 243–258.

25 Y. Hojo, T. Saito and H. Kondo, Role of apoptosis in left ventricular remodeling after acute myocardial infarction, *J. Cardiol.*, 2012, **60**, 91–92.

26 V. P. Van Empel, A. T. Bertrand, L. Hofstra, H. J. Crijns, P. A. Doevendans and L. J. De Windt, Myocyte apoptosis in heart failure, *Cardiovasc. Res.*, 2005, **67**, 21–29.

27 G. Häcker and S. A. Paschen, Therapeutic targets in the mitochondrial apoptotic pathway, *Expert Opin. Ther. Targets*, 2007, **11**, 515–526.

28 S. W. Chi, Structural insights into the transcription-independent apoptotic pathway of p53, *BMB Rep.*, 2014, **47**, 167–172.